Acetylcholinesterase Complexed with Bivalent Ligands Related to Huperzine A: Experimental Evidence for Species-Dependent Protein–Ligand Complementarity

ARTICLE *in* JOURNAL OF THE AMERICAN CHEMICAL SOCIETY · JANUARY 2003

Impact Factor: 12.11 · DOI: 10.1021/ja021111w · Source: PubMed

8 AUTHORS, INCLUDING:

Dawn M Wong
Virginia Polytechnic Institute and State Univ…
20 PUBLICATIONS **484** CITATIONS
SEE PROFILE

Harry M Greenblatt
Weizmann Institute of Science
46 PUBLICATIONS **1,597** CITATIONS
SEE PROFILE

Hay Dvir
28 PUBLICATIONS **1,368** CITATIONS
SEE PROFILE

Joel Sussman
Weizmann Institute of Science
359 PUBLICATIONS **22,958** CITATIONS
SEE PROFILE

J|A|C|S
ARTICLES
Published on Web 12/13/2002

Acetylcholinesterase Complexed with Bivalent Ligands Related to Huperzine A: Experimental Evidence for Species-Dependent Protein−Ligand Complementarity

Dawn M. Wong,[†,‡] Harry M. Greenblatt,[†] Hay Dvir,[†,‡] Paul R. Carlier,[§] Yi-Fan Han,[||] Yuan-Ping Pang,[⊥] Israel Silman,[‡] and Joel L. Sussman*[,†]

Contribution from Department of Structural Biology, Weizmann Institute of Science, Rehovot 76100, Israel, Department of Neurobiology, Weizmann Institute of Science, Rehovot 76100, Israel, Department of Chemistry, Virginia Tech, Blacksburg, Virginia 24061, Department of Biochemistry, Hong Kong University of Science and Technology, Clear Water Bay, Kowloon, Hong Kong, China, and Department of Molecular Pharmacology and Experimental Therapeutics, Mayo Foundation for Medical Education and Research, 200 First St. SW, Rochester, Minnesota 55905

Received August 22, 2002; E-mail: joel.sussman@weizmann.ac.il

Abstract: Acetylcholinesterase (AChE) inhibitors improve the cognitive abilities of Alzheimer patients. (−)-Huperzine A [(−)-HupA], an alkaloid isolated from the club moss, *Huperzia serrata*, is one such inhibitor, but the search for more potent and selective drugs continues. Recently, alkylene-linked dimers of 5-amino-5,6,7,8-tetrahydroquinolinone (hupyridone, **1a**), a fragment of HupA, were shown to serve as more potent inhibitors of AChE than (−)-HupA and monomeric **1a**. We soaked two such dimers, (*S*,*S*)-(−)-bis(10)-hupyridone [(*S*,*S*)-(−)-**2a**] and (*S*,*S*)-(−)-bis(12)-hupyridone [(*S*,*S*)-(−)-**2b**] containing, respectively, 10 and 12 methylenes in the spacer, into trigonal *Tc*AChE crystals, and solved the X-ray structures of the resulting complexes using the difference Fourier technique, both to 2.15 Å resolution. The structures revealed one HupA-like **1a** unit bound to the "anionic" subsite of the active-site, near the bottom of the active-site gorge, adjacent to Trp84, as seen for the *Tc*AChE/(−)-HupA complex, and the second **1a** unit near Trp279 in the "peripheral" anionic site at the top of the gorge, both bivalent molecules thus spanning the active-site gorge. The results confirm that the increased affinity of the dimeric HupA analogues for AChE is conferred by binding to the two "anionic" sites of the enzyme. Inhibition data show that (−)-**2a** binds to *Tc*AChE ∼6−7- and > 170-fold more tightly than (−)-**2b** and (−)-HupA, respectively. In contrast, previous data for rat AChE show that (−)-**2b** binds ∼3- and ∼2-fold more tightly than (−)-**2a** and (−)-HupA, respectively. Structural comparison of *Tc*AChE with rat AChE, as represented by the closely related mouse AChE structure (1maa.pdb), reveals a narrower gorge for rat AChE, a perpendicular alignment of the Tyr337 ring to the gorge axis, and its conformational rigidity, as a result of hydrogen bonding between its hydroxyl group and that of Tyr341, relative to *Tc*AChE Phe330. These structural differences in the active-site gorge explain the switch in inhibitory potency of (−)-**2a** and **2b** and the larger dimer/(−)-HupA potency ratios observed for *Tc*AChE relative to rat AChE. The results offer new insights into factors affecting protein−ligand complementarity within the gorge and should assist the further development of improved AChE inhibitors.

Introduction

Acetylcholinesterase inhibitors are thus far the only drugs approved for symptomatic treatment of Alzheimer's disease (AD).[1] According to the "cholinergic hypothesis", they prolong the effects of the endogenously released neurotransmitter, acetylcholine (ACh), by inhibiting the enzyme acetylcholinesterase (AChE, EC 3.1.1.7), thereby improving the cognitive abilities of early stage AD patients.[2,3] These drugs include synthetic compounds, such as tacrine (Cognex),[4,5] E2020 (Aricept),[6−8] and rivastigmine (Exelon).[9] However, their useful-

[†] Department of Structural Biology, Weizmann Institute of Science.
[‡] Department of Neurobiology, Weizmann Institute of Science.
[§] Department of Chemistry, Virginia Tech.
[||] Department of Biochemistry, Hong Kong University of Science and Technology.
[⊥] Department of Molecular Pharmacology and Experimental Therapeutics, Mayo Foundation for Medical Education and Research.

(1) Abbreviations: ACh, acetylcholine; AChE, acetylcholinesterase (EC 3.1.1.7); ATC, acetylthiocholine; AD, Alzheimer's disease; BChE, butyrylcholinesterase; BSA, bovine serum albumin; BW, BW284C51; ChE, cholinesterase; CNS, Crystallography & NMR System; DECA, decamethonium; DTNB, 5,5′-dithiobis(2-nitrobenzoic acid); Fas2, fasciculin-II; FBS, fetal bovine serum; hAChE, human AChE; (−)-HupA, (−)-huperzine A; IB, individual B-factor; MES, 2-[*N*-morpholino]ethanesulfonic acid; mAChE, mouse AChE; NAG, *N*-acetyl-D-glucosamine; NDG, 2-(acetylamino)-2-deoxy-α-D-glucopyranose; PDB, Protein Data Bank; PEG200, poly(ethylene glycol) 200; rmsd, root-mean-square deviation; SA, simulated annealing; STD, standard deviation; *Tc*, *Torpedo californica*; hupyridone, 5-amino-5,6,7,8-tetrahydroquinolinone; (*S*, *S*)−(−)-**2a**, (*S*,*S*)−(−)-*N*,*N*′-di-5′-[5′,6′,7′,8′-tetrahydro-2′(1′H)-quinolinonyl]-1,10-diaminodecane or (*S*,*S*)−(−)-bis(10)-hupyridone dihydrochloride; (*S*,*S*)−(−)-**2b**, (*S*,*S*)−(−)-*N*,*N*′-di-5′-[5′,6′,7′,8′-tetrahydro-2′(1′H)-quinolinonyl]-1,12-diaminododecane or (*S*,*S*)−(−)-bis(12)-hupyridone dihydrochloride; TMTFA, *m*-(*N*,*N*,*N*-trimethylammonio)-2,2,2-trifluoroacetophenone.

10.1021/ja021111w CCC: $25.00

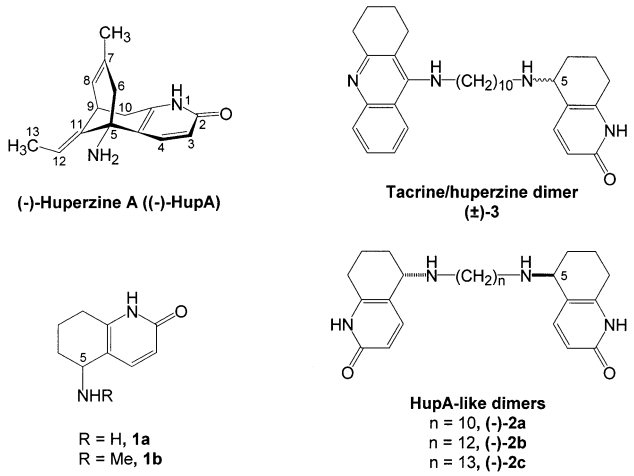

Figure 1. Chemical structures of the principal AChE inhibitors referred to in this study.

ness is limited by dose-dependent hepatotoxicity (tacrine) and by peripheral side effects. Two naturally occurring alkaloids have also been used clinically: (−)-galanthamine, marketed as Reminyl,[10,11] and (−)-huperzine A ((−)-HupA) (Figure 1) isolated from the club moss and Chinese medicinal herb, *Huperzia serrata*.[12,13] Lack of patent protection has effectively discouraged development of (−)-HupA as a prescription or over-the-counter pharmaceutical, and it is currently marketed as a nutraceutical memory enhancer.

The three-dimensional (3D) structure of AChE from *Torpedo californica* electric organ (*Tc*AChE) determined in 1991 provided valuable insights for studying structure−function relationships.[14] The active-site lies at the bottom of a deep narrow gorge (20 Å), named the "active-site gorge" or "aromatic gorge" because a substantial portion (almost 70%) is lined by the rings of 14 conserved aromatic amino acids.[15] At the "anionic" subsite of the active-site, modeling suggested that the quaternary amino group of ACh binds to the indole side chain of the conserved residue, Trp84, in a cation-π interaction,[16] as was subsequently demonstrated for the edrophonium (EDR), tacrine (THA), and *m*-(*N*,*N*,*N*-trimethylammonio)-2,2,2-trifluoroacetophenone (TMTFA) complexes with *Tc*AChE.[17,18] The complexes of *Tc*AChE with such bisquaternary ligands as decamethonium (DECA, $Me_3N^+(CH_2)_{10}NMe_3^+$)[17] and BW284C51 (BW),[19] led to the assignment of Trp279 as the major element of a second, remote binding site, near the top of the active-site gorge, named the peripheral "anionic" site, ∼14 Å from the active-site.[16,17,19] These structural assignments were borne out by a large body of biochemical studies, involving site-directed mutagenesis, which confirmed the important role of aromatic amino acid residues in AChE proposed on the basis of the crystallographic data.[20]

In an effort to improve drug potency and selectivity, the bivalent ligand strategy was applied to the development of AChE-targeted therapeutic agents. The heptylene-linked tacrine dimer, bis(7)-tacrine, was synthesized and evaluated after computational studies predicted weak affinity of tacrine for the peripheral "anionic" site residues, Trp279 and Tyr70 in *Tc*AChE,[21] in conjunction with high affinity of tacrine for the X-ray-identified catalytic 'anionic' site (Trp84 and Phe330 in *Tc*AChE).[17] Subsequent studies of bistacrine with alkyl spacers of varying lengths confirmed that bis(7)-tacrine possessed both optimum AChE inhibition potency and AChE/butyrylcholinesterase (BChE) selectivity; bis(7)-tacrine showed significantly higher potency and selectivity for inhibition of rat AChE than monomeric tacrine.[22,23] The superior inhibitory capacity of bis(7)-tacrine relative to tacrine is attributed to dual-site binding and operation of the chelate effect.[24] Studies of related ligands on rat AChE also demonstrated beneficial hydrophobic effects imparted by the alkylene tether to the peripheral site ligand.[25,26] The recently reported increased affinity for electric eel AChE of bivalent (−)-galanthamine derivatives,[27] and of a tacrine/propidium heterodimer,[28] supports design and modification of drugs with dual-site binding properties.

One important observation made during application of the "bivalent strategy" to AChE inhibitor design was that drug units that have little or no intrinsic affinity for AChE can function as effective catalytic and/or peripheral site ligands when incorporated into a bivalent drug.[25,26] On the basis of docking studies which indicated affinity of (−)-HupA for both the catalytic and peripheral binding sites in AChE,[21] dimerization of an easily synthesized but pharmacologically inactive fragment of (−)-HupA, hupyridone, a simplified HupA-like monomer (**1a**; Figure 1), was performed. The optimum dimers (*S*,*S*)-(−)-bis(12)-hupyridone [(*S*,*S*)-(−)-**2b**] and (*S*,*S*)-(−)-bis(13)-hupyridone [(*S*,*S*)-(−)-**2c**] (linked by 12 and 13 methylenes respectively, Figure 1) proved to be >2-fold as potent as the natural product, (−)-HupA, on rat AChE.[29] Although the optimal HupA-like

(2) Bartus, R. T.; Dean, R. L.; Beer, B.; Lippa, A. S. *Science* **1982**, *217*, 408−414.
(3) Giacobini, E. In *Cholinesterases and Cholinesterase Inhibitors*; Giacobini, E., Eds.; Martin Dunitz Ltd: London, 2000; pp 181−226.
(4) Watkins, P. B.; Zimmerman, H. J.; Knapp, M. J.; Gracon, S. I.; Lewis, K. W. *J. Am. Med. Assoc.* **1994**, *271*, 992−998.
(5) Davis, K. L.; Powchik, P. *Lancet* **1995**, *345*, 625−630.
(6) Nightingale, S. L. *J. Am. Med. Assoc.* **1997**, *277*, 10.
(7) Kawakami, Y.; Inoue, A.; Kawai, T.; Wakita, M.; Sugimoto, H.; Hopfinger, A. J. *Bioorg. Med. Chem. Lett.* **1996**, *4*, 1429−1446.
(8) Kryger, G.; Silman, I.; Sussman, J. L. *Structure* **1999**, *7*, 297−307.
(9) Bar-On, P.; Millard, C. B.; Harel, M.; Dvir, H.; Enz, A.; Sussman, J. L.; Silman, I. *Biochemistry* **2002**, *41*, 3555−3564.
(10) Harvey, A. L. *Pharmacol. Ther.* **1995**, *68*, 113−128.
(11) Greenblatt, H. M.; Kryger, G.; Lewis, T.; Silman, I.; Sussman, J. L. *FEBS Lett.* **1999**, *463*, 321−326.
(12) Raves, M. L.; Harel, M.; Pang, Y.-P.; Silman, I.; Kozikowski, A. P.; Sussman, J. L. *Nature Struct. Biol.* **1997**, *4*, 57−63.
(13) Tang, X. C.; Han, Y.-F. *CNS Drug Rev.* **1999**, *5*, 281−300.
(14) Sussman, J. L.; Harel, M.; Frolow, F.; Oefner, C.; Goldman, A.; Toker, L.; Silman, I. *Science* **1991**, *253*, 872−879.
(15) Axelsen, P. H.; Harel, M.; Silman, I.; Sussman, J. L. *Protein Sci.* **1994**, *3*, 188−197.
(16) Ma, J. C.; Dougherty, D. A. *Chem. Rev.* **1997**, *97*, 1303−1324.
(17) Harel, M.; Schalk, I.; Ehret-Sabatier, L.; Bouet, F.; Goeldner, M.; Hirth, C.; Axelsen, P.; Silman, I.; Sussman, J. L. *Proc. Natl. Acad. Sci. U.S.A.* **1993**, *90*, 9031−9035.
(18) Silman, I.; Millard, C. B.; Ordentlich, A.; Greenblatt, H. M.; Harel, M.; Barak, D.; Shafferman, A.; Sussman, J. L. *Chem. Biol. Interactions* **1999**, *119*−*120*, 43−52.
(19) Felder, C. E.; Harel, M.; Silman, I.; Sussman, J. L. *Acta Crystallogr.* **2002**, *D58*, 1765−1771.
(20) Taylor, P.; Radic, Z. *Annu. Rev. Pharmacol. Toxicol.* **1994**, *34*, 281−320.
(21) Pang, Y.-P.; Kozikowski, A. *J. Comput.-Aided Mol. Des.* **1994**, *8*, 669−681.
(22) Pang, Y.-P.; Quiram, P.; Jelacic, T.; Hong, F.; Brimijoin, S. *J. Biol. Chem.* **1996**, *271*, 23 646−23 649.
(23) Carlier, P. R.; Han, Y.-F.; Chow, E. S.-H.; Li, C. P.-L.; Wang, H.; Lieu, T. X.; Wong, H. S.; Pang, Y.-P. *Bioorg. Med. Chem.* **1999**, *7*, 351−357.
(24) Jencks, W. P. *Proc. Natl. Acad. Sci. U.S.A.* **1981**, *78*, 4046−4050.
(25) Carlier, P. R.; Chow, E. S.-H.; Han, Y.-F.; Jing Liu, J.; El Yazal, J.; Pang, Y.-P. *J. Med. Chem.* **1999**, *42*, 4225−4231.
(26) Han, Y.-F.; Li, C. P.-L.; Chow, E.; Wang, H.; Pang, Y.-P.; Carlier, P. R. *Bioorg. Med. Chem. Lett.* **1999**, *7*, 2569−2575.
(27) Mary, A.; Renko, D. Z.; Guillou, C.; Thal, C. *Bioorg. Med. Chem. Lett.* **1998**, *6*, 1835−1850.
(28) Lewis, W. G.; Green, L. G.; Grynszpan, F.; Radic, Z.; Carlier, P. R.; Taylor, P.; Finn, M. G.; Sharpless, K. B. *Angew. Chem., Int. Ed.* **2002**, *41*, 1053−1057.
(29) Carlier, P. R.; Du, D.-M.; Han, Y.-F.; Liu, J.; Perola, E.; Williams, I. D.; Pang, Y.-P. *Angew. Chem., Int. Ed.* **2000**, *39*, 1775−1777.

dimers are not as potent as bis(7)-tacrine[23] or the tacrine/huperzine fragment heterodimer (±)-**3**[25] on rat AChE (IC_{50}), they are superior to the latter dimers in terms of selectivity for AChE: (*S*,*S*)-(−)-**2b** and (*S*,*S*)-(−)-**2c** are 185- and 321-fold more potent, respectively, for rat AChE than for BChE.[29] Interestingly, whereas the potent enantiomer of huperzine A, (−)-HupA, is (*R*)-configured at C-5, the potent enantiomers of **2b** and **2c** are (*S*,*S*)-configured. In both cases, the degree of enantiopreference is similar: 35-fold (*Tc*AChE) to 88-fold (FBS AChE) for (−)-HupA,[30] and 60-fold for **2b** (rat AChE).[29] The difference in preferred absolute stereochemistry raises the question of whether the catalytic site unit of (*S*,*S*)-(−)-**2b**/**2c** binds to the enzyme similarly to (−)-HupA. Docking studies of (*R*)- and (*S*)-**1b** (protonated at the amino group) with *Tc*AChE indicated tighter binding of the (*R*)-enantiomer, just as for (−)-HupA.[29] The docking studies also reveal that the amino group of (*R*)-**1b** does not easily accommodate an alkylene tether leading upward toward the peripheral site; in contrast, (*S*)-**1b** encounters no such problem.[29] On the basis of the docking studies, it would appear that the dimeric nature of **2b**/**2c** plays a role in the reversed enantioselection.[29] The recently solved structure of the *Tc*AChE/(+)-HupA complex,[31] which shows the weaker affinity (*S*)-enantiomer, (+)-HupA, binding at the catalytic site in an orientation similar to that of (−)-HupA,[12] lends further support to this hypothesis.

Although computerized docking protocols provide likely binding sites and ligand orientations in AChE,[21] determination of the 3D structures of the appropriate ligand-AChE complexes provides the only secure method for understanding the structural determinants of affinity for inhibitors, as was seen for (−)-HupA and (+)-HupA,[12,31] E2020,[8] (−)-galanthamine,[11] fasciculin-II (Fas2),[32] and the tacrine/huperzine hybrid, huprine X.[33] Furthermore, knowledge of the binding mode of (*S*,*S*)-(−)-**2b** would confirm whether it binds to the catalytic site similarly to (−)-HupA, and would permit structure−function studies for this potential AD drug candidate, thus facilitating further drug development. For these reasons, we sought to determine the 3D structure of the complexes of the optimum dimer, (*S*,*S*)-(−)-**2b**, and of its less potent homolog, (*S*,*S*)-(−)-**2a**, with *Tc*AChE to evaluate the structural features contributing to the inhibitory differences seen for rat AChE (IC_{50} = 52 nM and 151 nM for (*S*,*S*)-(−)-**2b** and (*S*,*S*)-(−)-**2a**, respectively; Figure 1).[29] Because Phe330 in *Tc*AChE is replaced by Tyr at position 337 in human AChE (hAChE), FBS, mouse and rat AChEs,[34−36] we considered it essential to obtain steady-state kinetic data for inhibition of *Tc*AChE by (*S*,*S*)-(−)-**2a** and **2b** to confirm our structure−activity correlations. Below we present the X-ray crystal structures of the complexes *Tc*AChE/(*S*,*S*)-(−)-**2a** and *Tc*AChE/(*S*,*S*)-(−)-**2b**, both at 2.15 Å resolution, and study the inhibition by both dimers and by (−)-HupA of *Tc*AChE and rat AChE.[37]

Experimental Section

Inhibitors. (−)-HupA (>99% pure by NMR, from Alexis Corporation, batch L00969) was used as supplied. Ligands (−)-**2a** (dihydrochloride salt, 98 area% pure by HPLC) and (−)-**2b** (dihydrochloride salt, 95 area% pure by HPLC) were prepared as described previously.[29]

Other Chemicals. Acetylthiocholine iodide (ATC), bovine serum albumin (BSA), 5,5′-dithiobis(2-nitrobenzoic acid) (DTNB; Ellman's reagent), 2-[*N*-morpholino]ethanesulfonic acid (MES), and poly(ethylene glycol) 200 (PEG200) were all purchased from Sigma Chemicals (St Louis, MO).

Purification and Crystallization of *Tc*AChE. The membrane-bound dimeric form of *Tc*AChE was solubilized with phosphatidylinositol-specific phopholipase C. It was then purified by affinity chromatography as decribed,[38] but with one modification: tetramethylammonium bromide was used instead of decamethonium bromide to elute the enzyme from the affinity column.[12] A stock solution of the enzyme at 10.2−10.9 mg/mL in dialysis buffer (1 mM MES, pH 6.5, containing 100 mM NaCl and 0.02% (w/v) NaN_3), was used for crystallization. *Tc*AChE crystals were obtained using the hanging-drop vapor diffusion method.[39] The protein stock solution (3 μL), was mixed with a solution of 40% (v/v) PEG200 in 0.5 M MES, pH 5.8 (3 μL) and set over a well solution of 28−30% (v/v) PEG200 in 0.5 M MES, pH 5.8 (500 μL). The 6 μL mixed drops were equilibrated for 3 h at 4 °C. Using a cat's whisker that had been dipped in a drop (100 μL) containing 10% dialysis buffer, 10% 0.5 M MES, pH 5.8, 40% water, 40% PEG200 (v/v/v/v), and crushed native trigonal crystals,[12] the mixed drops were seeded and left at 4 °C. Trigonal crystals of *Tc*AChE grew within a few weeks. The crystalline complex with (−)-**2a** was obtained by soaking native *Tc*AChE crystals at 4 °C in mother liquor (40% (v/v) PEG200 in 0.1 M MES, pH 5.8, 6 μL drop) containing 2 mM (−)-**2a** for 1 d. Crystalline *Tc*AChE/(−)-**2b** was similarly obtained using a 10 mM solution of (−)-**2b** for 2 d.

Enzymatic Assays. ATC was used as the substrate for AChE. After preincubation of the enzyme with the appropriate inhibitor (25 min for (−)-HupA, 2 h for (−)-**2a**, and 4 h for (−)-**2b**), the reaction was initiated by adding substrate, and rates were obtained from initial velocities (v). Activity was followed by the spectrophotometric procedure of Ellman et al.[40] at 405 nm, with 0.3 mM DTNB. The reaction mixture contained 270 μL phosphate buffer (10 mM Na_2HPO_4/NaH_2PO_4, pH 7.0, containing 50 mM NaCl, 0.01 mg/mL BSA and 0.02% (w/v) NaN_3), 35 μL of inhibitor solution in the same buffer, and 35 μL of substrate dissolved in water. Inhibitor concentrations were determined from their absorbance at λ_{max} using the following molar extinction coefficients: ϵ_{312nm} = 7762 M^{-1} cm^{-1} for (−)-HupA;[41] ϵ_{302nm} = 14 566 M^{-1} cm^{-1} for (−)-**2b**. Concentrations for (−)-**2a** were determined using the same absorbance λ_{max} and molar extinction coefficient as for (−)-**2b**. Activity was monitored on a TECAN Spectra Fluor Plus (Durham NC) microplate reader at room temperature (~25 °C), with 3−5 repeats, and was corrected for spontaneous substrate hydrolysis. A final enzyme concentration of ca. 40 pM yielded a reaction rate of ca. 0.06 ΔA/min, using 0.5 mM substrate in the absence of inhibitor. To preclude substrate inhibition, substrate concentrations (s) were <0.5 mM. The steady-

(30) Saxena, A.; Qian, N.; Kovach, I. M.; Kozikowski, A. P.; Pang, Y.-P.; Vellom, D. C.; Radic, Z.; Quinn, D.; Taylor, P.; Doctor, B. P. *Protein Sci.* **1994**, *3*, 1770−1778.
(31) Dvir, H.; Jiang, H. L.; Wong, D. M.; Harel, M.; Chetrit, M.; He, X. C.; Tang, X. C.; Silman, I.; Bai, D. L.; Sussman, J. L. *Biochemistry* **2002**, *41*, 10 810−10 818.
(32) Harel, M.; Kleywegt, G. J.; Ravelli, R. B. G.; Silman, I.; Sussman, J. L. *Structure* **1995**, *3*, 1355−1366.
(33) Dvir, H.; Wong, D. M.; Harel, M.; Barril, X.; Orozco, M.; Luque, F. J.; Muñoz-Torrero, D.; Camps, P.; Rosenberry, T. L.; Silman, I.; Sussman, J. L. *Biochemistry* **2002**, *41*, 2970−2981.
(34) Gentry, M. K.; Doctor, B. P. In *Cholinesterases: Structure, Function, Mechanism, Genetics and Cell Biology*; Massoulié, J., Bacou, F., Barnard, E., Chatonnet, A., Doctor, B. P., Quinn, D. M., Eds.; American Chemical Society: Washington, DC, 1991; pp 394−398.
(35) Massoulié, J.; Sussman, J. L.; Doctor, B. P.; Soreq, H.; Velan, B.; Cygler, M.; Rotundo, R.; Shafferman, A.; Silman, I.; Taylor, P. In *Multidisciplinary Approaches to Cholinesterase Functions;* Shafferman, A., Velan, B., Eds.; Plenum Press: New York, 1992; pp 285−288.
(36) Cousin, X.; Hotelier, T.; Giles, K.; Toutant, J. P.; Chatonnet, A. *Nucl. Acids Res.* **1998**, *26*, 226−228.
(37) Henceforth, compounds (*S*,*S*)-(−)-**2a** and (*S*,*S*)-(−)-**2b** will be referred to as (−)-**2a** and (−)-**2b** respectively.
(38) Sussman, J. L.; Harel, M.; Frolow, F.; Varon, L.; Toker, L.; Futerman, A. H.; Silman, I. *J. Mol. Biol.* **1988**, *203*, 821−823.
(39) McPherson, A. *Methods Biochem. Anal.* **1976**, *23*, 249−345.
(40) Ellman, G. L.; Courtney, K. D.; Andres, V.; Featherstone, R. M. *Biochem. Pharmacol.* **1961**, *7*, 88−95.
(41) Liu, J.-S.; Zhu, Y.-L.; Yu, C.-M.; Zhou, Y.-Z.; Han, Y.-Y.; Wu, F.-W.; Qi, B.-F. *Can. J. Chem.* **1986**, *64*, 837−839.

Table 1. AChE Inhibition Parameters of (−)-**2a**, (−)-**2b** and (−)-HupA

	*Tc*AChE		Rat cortex AChE[a]	
inhibitor	$K_i \pm \sigma$ (nM) [b]	$IC_{50} \pm \sigma$(nM)	K_i (nM)	$IC_{50} \pm \sigma$(nM)
(−)-**2a**	0.8 ± 0.1[c]	2.4 ± 0.1		151 ± 36
(−)-**2b**	4.5 ± 0.4[c]	16.0 ± 0.6	19.6[d]	52 ± 8
(−)-HupA	175 ± 17[c,e]	414 ± 48	47.1[c]	114 ± 1
inhibition ratios				
(−)-HupA/(−)-**2a**	∼233	∼173		0.8
(−)-HupA/(−)-**2b**	∼39	∼26	2.4	2.2
(−)-**2b**/(−)-**2a**	∼6	∼7		0.3

[a] Values reported previously using rat cortex homogenates.[29] K_i values determined from analysis of slopes of $1/v$ vs $1/s$ plots at various [I]. [b] K_i values for *Tc*AChE were determined from analysis of linearly fitted K_{app}/V_{maxi} values vs [I] plots (Figure 3), as previously described.[33] [c] Linear-mixed type inhibition. [d] Noncompetitive type inhibition. [e] Values reported previously under identical conditions.[31]

state inhibition data for all the inhibitors were treated as previously reported, and the modes of inhibition and the dissociation constant, K_i, for AChE inhibition were obtained as described;[33] the terms V_{max}, K_m, V_{maxi}, and K_{app} were defined previously.[33] The activities were also compared to the activity of a drug-free control and expressed as a percent of activity. IC_{50} values were determined at 0.2 mM total substrate concentration from a plot of percent enzyme activity versus −log[I], where [I] refers to inhibitor concentration. The presented values are the averages of three determinations. Standard errors are < 12% of the mean IC_{50} values (see Table 1).

X-ray Data Collection. Crystals were transferred to oil (Paratone, EXXON)[42] for cryo-protection, mounted on a nylon cryo-loop, placed on the goniostat and flash cooled to 120 K in an Oxford Systems Cryostream. The X-ray source was a Rigaku RU−H3R rotating anode, employing a copper target set at 50 kV/90 mA for the (−)-**2a** and 50 kV/100 mA for the (−)-**2b** complex, at $\lambda = 1.5418$ Å (Cu K_α). Images were collected using a Rigaku R-AXIS IV++ image plate area detector.

Data collection was optimized by the program STRATEGY.[43] Data processing was performed with DENZO and SCALEPACK.[44] Data were truncated with the CCP4 program TRUNCATE,[45] and a list of 5% randomly generated test reflections was used from a master list for the trigonal crystal form of *Tc*AChE using CAD and FREEFLAG.[45] Reflections were output with MTZ2VARIOUS[45] to a format suitable for the CNS_SOLVE package (version 1.0).[46] Table 2 summarizes pertinent information concerning X-ray data collection and processing.

Structure Determination and Refinement. The structures of both the *Tc*AChE/(−)-**2a** and *Tc*AChE/(−)-**2b** complexes were solved using the difference Fourier technique, exploiting the native isomorphous crystal structure of *Tc*AChE (PDB ID code 2ACE).[12] Unless otherwise stated, all refinement was done using CNS, employing the Engh and Huber parameters.[47] All data with B-correction from 6 to 2.15 Å resolution were used in the refinement, and maps were calculated using all data ($F > 0\sigma$) in the 30−2.15 Å resolution range. The 2ACE coordinates were used as a starting model for refinement, initially by rigid body refinement (30−2.15 Å resolution for (−)-**2a**; 30−2.4 Å resolution for (−)-**2b**). Subsequently, difference maps (Fo−Fc) and 2Fo−Fc maps were calculated, and used to fit the inhibitors, two carbohydrate moieties and water molecules (40 waters for (−)-**2a**, and 69 for the (−)-**2b** complex initially). Using the previously generated pseudoaxial (i.e., at C-5) and pseudoequatorial conformations of (*S*)-**1a**·H^+ and (*S*)-**1b**·H^+,[29] it was found that the pseudoaxial conformation best fitted the initial ligand electron densities near the peripheral "anionic" site, and that the pseudoequatorial conformation best fitted the initial ligand electron densities near the bottom of the active-site gorge, in both complex structures. Chemical models of the inhibitors (−)-**2a** and (−)-**2b** (PDB format) were then built with one monomer (*S*)-**1a** unit pseudoaxial and the other with a pseudoequatorial conformation, using CS Chem3D Pro (version 5.0).[48] Energy minimization was performed on the inhibitor models, using the molecular dynamics utilities of CS Chem3D Pro.[48] These models were, in turn, used to generate suitable topology and parameter files for CNS using AUTODIC from the XPLO2D program (version 001221/2.8.9)[49] prior to map fitting. The respective (*S*)-**1a** units and part of the alkylene linker (three carbons) were initially modeled into the two largest positive peaks of the initial Fo−Fc difference maps, corresponding to the two AChE binding sites as described above. As the map phases improved with subsequent refinements, the linker chain was gradually built into the ligand electron density and additional water molecules were added (Figure 2). Changes to the Gly117−Gly118 peptide bond and Phe330 side chain were made to fit the 2Fo−Fc maps, as well as a few minor changes to side chains outside the active-site. The program XtalView (version 4.0)[50] was used for all model building, and X-ray crystal structures of *Tc*AChE and of its complexes were compared using LSQMAN (version 010126/7.7.1).[51]

Simulated annealing (SA, torsion dynamics mode)[52] at 2500 K with harmonic constraints for individual atoms was then carried out, followed by individual B-factor (IB) refinements using CNS. The models were further refined by several cycles of positional maximum-likelihood minimization, followed by IB refinement,[46] until the R-factors converged (see Table 3 for summarized results). Two alternate side chain conformations were fitted for residues Leu143 (set to 50% occupancy each) and Arg243 (set to 80% and 20% occupancy) in the *Tc*AChE/(−)-**2a** structure. A total of 222 and 269 water molecules were fitted for the (−)-**2a** and (−)-**2b** complex structures, respectively. Finally, simulated annealed omit Fo−Fc maps (SA at 1000 K, torsion dynamics mode) were generated for the refined structures, with the ligand atoms omitted from the map calculations. The maps show electron density for the complete inhibitors in the gorge of *Tc*AChE, indicating that no model bias was used during fitting and refinement. The coordinates of both refined structures and the corresponding structure factors have been submitted to the PDB (ID Codes 1H22 for *Tc*AChE/(−)-**2a** and 1H23 for *Tc*AChE/(−)-**2b**). Pictures of the X-ray structures were made with Xfit[50] and Raster3D.[53]

Results

Inhibition of *Tc*AChE. Steady-state measurements of *Tc*AChE activity in the presence of (−)-**2a**, (−)-**2b**, and (−)-HupA reveal that all three exhibit linear-mixed type inhibition, where the V_{maxi} values (values of V_{max} at a given inhibitor concentration [I]) decrease as a function of [I], whereas the corresponding K_{app} values (observed K_m values at [I]) increase with [I] (data not shown). The K_{app}/V_{maxi} values were linearly dependent on [I] for all three compounds (Figure 3). K_i values obtained from the slopes of the linear fitted lines in Figure 3 are presented in Table 1. The averaged IC_{50} values determined from independent plots of percent AChE activity versus −log[I] are also presented in Table 1.

(42) Hope, H. *Acta Crystallogr.* **1988**, *B44*, 22−26.
(43) Ravelli, R. B. G.; Sweet, R. M.; Skinner, J. M.; Duisenberg, A. J. M.; Kroon, J. *J. Appl. Crystallogr.* **1997**, *30*, 551−554.
(44) Otwinowski, Z.; Minor, W. *Methods Enzymol.* **1997**, *276*, 307−326.
(45) Bailey, S. *Acta Crystallogr.* **1994**, *D50*, 760−763.
(46) Brünger, A. T.; Adams, P. D.; Clore, G. M.; DeLano, W. L.; Gros, P.; Grosse-Kunstleve, R. W.; Jiang, J. S.; Kuszewski, J.; Nilges, M.; Pannu, N. S.; Read, R. J.; Rice, L. M.; Simonson, T.; Warren, G. L. *Acta Crystallogr.* **1998**, *D54*, 905−921.
(47) Engh, R. A.; Huber, R. *Acta Crystallogr.* **1991**, *A47*, 392−400.
(48) CambridgeSoft **1999**; *CS Chem3D Pro*, 5.0 ed.; CambridgeSoft Corporation, 100 Cambridge Park Dr., Cambridge, MA 02140-2317, USA, http://www.camsoft.com.
(49) Kleywegt, G. J.; Jones, T. A. *Methods Enzymol.* **1997**, *277*, 208−230, http://xray.bmc.uu.se/gerard/gmrp/gmrp.html.
(50) McRee, D. E. *J. Struct. Biol.* **1999**, *125*, 156−165.
(51) Kleywegt, G. J.; Jones, T. A. *ESF/CCP4 Newsletter* **1994**, *31*, November, 9−14, http://xray.bmc.uu.se/usf/factory_4.html.
(52) Brünger, A. T.; Adams, P. D.; Rice, L. M. *Prog. Biophys. Mol. Biol.* **1999**, *72*, 135−155.
(53) Merritt, E. A.; Bacon, D. J. *Methods Enzymol.* **1997**, *277*, 505−524.

Table 2. X-ray Data Collection and Processing

parameters	*Tc*AChE/(−)-**2a**	*Tc*AChE/(−)-**2b**
space group	$P3_121$	$P3_121$
cell axes (Å)	$a = b = 111.460$, $c = 137.337$	$a = b = 111.794$, $c = 137.775$
T (K)	120	120
oscillation angle (°)	0.5	0.5
total number of frames	120	142
resolution range (Å)	26.4−2.15	29.3−2.15
no. of measured reflections	447 124	536 295
no. of unique reflections	53 982	54 602
no. of unique reflections used	51 434	54 392
redundancy (% reflections)	0 (4.7), 1 (12.5), 2 (18.9), 3 (15.1), 4 (20.0), 5−6 (19.7), 7−8 (9.2)	0 (0.3), 1 (3.2), 2 (17.6), 3 (27.6), 4 (15.9), 5−6 (20.4), 7−8 (11.2), 9−12 (3.8)
completeness: all data (highest shell)[a]	95.3% (96.8%)	99.7% (99.8%)
R_{merge}: all data (highest shell)[a]	4.9% (22.8%)	6.6% (39.6%)
mean <I/sigma>: all data	17.3	13.5
reflections in highest resolution shell with I/sigma less than 3σ	47.3%	60.6%

[a] Highest resolution shell was 2.23−2.15 Å.

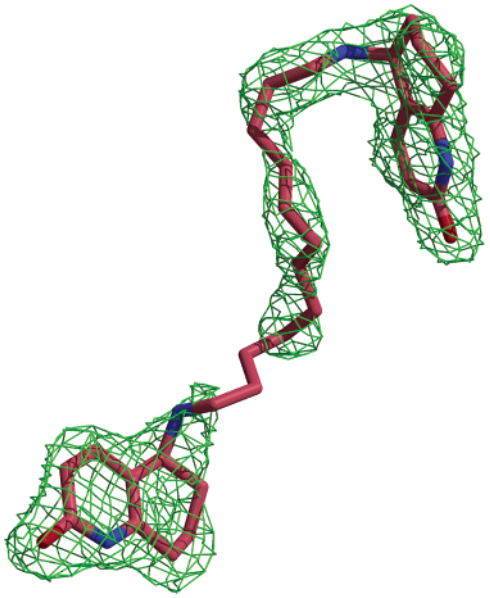

Figure 2. View of refined structure of (−)-**2b** (pink) in the active-site of *Tc*AChE displayed in the initial Fo-Fc map, at 2.15 Å resolution. Map, shown in thin green lines, is contoured at 3.0σ after refinement of the native protein coordinates (in the absence of the ligand; see Experimental Section).

The K_i values for *Tc*AChE show that the (−)-**2a** dimer is ca. 6- and 233-fold more potent than the longer C_{12}-linker homolog, (−)-**2b**, and (−)-HupA, respectively. Moreover, (−)-**2b** is ca. 39-fold more potent than (−)-HupA, and the dimer/(−)-HupA potency ratios are larger for *Tc*AChE than for rat AChE (Table 1).[29] The inhibitor potency ratios based on the IC_{50} values also correspond well with the K_i ratios, with dimer/(−)-HupA potency ratios of ca. 173 and 26 for (−)-**2a** and (−)-**2b**, respectively. In contrast, (−)-**2a** is the least potent inhibitor for rat AChE, exhibiting only ca. 0.3-fold and 0.8-fold the potency of (−)-**2b** and (−)-HupA, respectively. Furthermore, the IC_{50} results indicate that both dimers (−)-**2a** and (−)-**2b** are better inhibitors of *Torpedo* AChE than of rat AChE, with rat AChE/*Tc*AChE inhibition ratios of ca. 63 and 3, respectively. This species selectivity may be attributed to the presence of a Tyr residue at position 337 in mammalian AChE (mouse, human) in place of a Phe in *Tc*AChE (at the corresponding position 330),[36] as was previously suggested for (−)-HupA[30,54,55] and, more recently, for huprine X and tacrine.[33] The data also show that (−)-HupA inhibits rat AChE better than it does *Tc*AChE (ca. 4-fold). Although the magnitude of the reported difference varies depending upon experimental conditions, our present data conform to the trend previously reported for racemic and (−)-HupA interacting with *Tc*AChE, FBS AChE and hAChE,[30,54] mouse AChE (mAChE),[55] and mutant hAChE.[56]

Refinement and Map Fitting. X-ray data for trigonal crystals of *Tc*AChE soaked with either (−)-**2a** or (−)-**2b** (see Table 2) were collected and refined, both to 2.15 Å resolution (Table 3). From the initial Fo−Fc maps, calculated after the first cycle of refinement, the locations of the binding sites for (−)-**2a** and (−)-**2b** in the gorge of *Tc*AChE were readily identified as >5.5 σ peaks for the two HupA-like **1a** fragments of both dimers. In both cases, one **1a** unit (**1a**$_{cat}$) was seen adjacent to the indole ring of Trp84, near the bottom of the active-site gorge, viz. at the "anionic" subsite of the active-site, and the other **1a** unit (**1a**$_{per}$) was seen near the indole ring of Trp279 at the peripheral "anionic" site near the lip of the gorge.[17] The electron density due to the alkylene linker was mostly visible, and can be seen to snake along the gorge between the two **1a** moieties of the dimers, thus spanning the gorge (Figure 2). To ensure that there was no model bias, only part of the alkylene linker (3 carbons) was initially fitted into the initial Fo−Fc maps, which became clearer upon further model building and several cycles of refinement. Only the (*S*,*S*)-(−)-configurations of **2a** and **2b** could be modeled into the maps. Thus, the correct absolute configurations of the potent enantiomers of these dimers as assigned,[29] were confirmed by the 3D crystal structures of the complexes. Subsequently, two carbohydrate moieties[57] were modeled for two of the four putative glycosylation sites of *Tc*AChE (Asn59 and Asn416)[58] of both complexes. A total of 222 and 269 water molecules, respectively, were assigned to the structures of *Tc*AChE/(−)-**2a** and *Tc*AChE/(−)-**2b**. The R-factors decreased

(54) Ashani, Y.; Peggins, J. O., III.; Doctor, B. P. *Biochem. Biophys. Res. Commun.* **1992**, *184*, 719−726.
(55) Saxena, A.; Redman, A. M. G.; Jiang, X.; Lockridge, O.; Doctor, B. P. *Biochemistry* **1997**, *36*, 14 642−14 651.
(56) Ariel, N.; Ordentlich, A.; Barak, D.; Bino, T.; Velan, B.; Shafferman, A. *Biochem. J.* **1998**, *335*, 95−102.
(57) For complex *Tc*AChE/(−)-**2a** (1h22.pdb): two NAG groups (ref 1) were modeled to form β bonds between their C1 carbons and the amide nitrogens of Asn59 and Asn416; for complex *Tc*AChE/(−)-**2b** (1h23.pdb): one NDG and one NAG group (ref 1) were modeled to form β bonds between their C1 carbons and the amide nitrogens of Asn59 and Asn416, respectively.
(58) Schumacher, M.; Camp, S.; Maulet, Y.; Newton, M.; MacPhee-Quigley, K.; Taylor, S. S.; Friedmann, T.; Taylor, P. *Nature* **1986**, *319*, 407−409.

Table 3. Refinement and Model Statistics

	*Tc*AChE/(−)-**2a**	*Tc*AChE/(−)-**2b**
resolution range (Å)	26.4−2.15	29.3−2.15
number of reflections	51 401	54 357
R_{work}[a]	19.0%	18.9%
R_{free} (5% of reflections)[a]	22.1%	21.5%
no. of protein atoms	4,172	4,184
no. of nonprotein atoms		
solvent (water)	222	269
carbohydrate	28	28
inhibitor	34	36
B factor (Å^2): average/σ/min/max		
protein	34.0/7.4/21.1/70.6	34.4/8.0/20.5/68.8
water molecules	37.2/6.9/23.5/54.3	37.7/6.9/21.8/59.6
carbohydrate	54.7/7.4/44.0/65.1	56.4/7.8/45.5/67.2
inhibitor	34.3/4.4/29.5/45.2	35.3/4.9/28.7/44.2
RMS bond length deviation (Å)	0.022	0.020
RMS bond angle deviation (°)	1.95	1.94
agreement with Ramachandran plot[b]	89.8% in the most favorable region; two residues in the generously allowed region.	88.9% in the most favorable region; two residues in the generously allowed region.

[a] All the output reflections from TRUNCATE were used in the refinement, with no σ cutoff. [b] Analysis done with PROCHECK.[73]

continuously during refinement of both structures, and finally converged to the values given in Table 3.

The protein backbone in the *Tc*AChE/(−)-**2a** and *Tc*AChE/(−)-**2b** crystal structures were very similar to each other, with root-mean-square deviations (rmsd) for the main chain (C_α) carbon atoms of 0.11 Å (for 528 residues).[59] Such similarity is also observed between the native *Tc*AChE and *Tc*AChE/(−)-HupA structures previously reported (rmsd value of 0.18 Å (527) for PDB entries 2ACE and 1VOT, respectively). However, the overall crystal structures of both *Tc*AChE/dimer complexes, relative to either the native *Tc*AChE or to the *Tc*AChE/(−)-HupA complex deviate more substantially. Average rmsd values for the C_α atoms for the two dimers are 0.315 ± 0.001 Å (527) relative to native *Tc*AChE, and 0.313 ± 0.001 Å (527) relative to *Tc*AChE(−)-HupA.

All the protein residues in the vicinity of the bound (−)-**2a** and (−)-**2b** dimers, except for Phe330, have very similar conformations to those seen in the *Tc*AChE/(−)-HupA structure (PDB ID 1VOT) (Figure 4).[12] The conformation of the Phe330 ring in both dimer structures is aligned parallel to the gorge axis, with an orientation very similar to that observed in the *Tc*AChE/E2020 structure (PDB ID 1EVE),[8] the *Tc*AChE/(−)-galanthamine structure (PDB ID 1DX6),[11] and the *Tc*AChE/DECA structure (PDB ID 1ACL).[17] It is, however, significantly different from that observed in native *Tc*AChE, and in the complexes with (−)-HupA,[12] EDR (PDB ID 2ACK),[17] and BW (PDB ID 13EQ),[19] in which the Phe330 ring is rotated 90° and lies perpendicular to the gorge axis, with an orientation similar to that seen for the corresponding Tyr337 residue in the homologous mAChE structure, which also contains a bound DECA molecule in the gorge (PDB ID 1MAA).[60] The different orientations adopted by Phe330 in different complexes of *Tc*AChE appear to be dependent upon the ligand structure, the ability of the enzyme gorge to accommodate structurally diverse ligands, and different modes of interaction exhibited by Phe330 and other gorge residues. These include polar (cation-π, H-bond) and nonpolar (aromatic−aromatic, hydrophobic) interactions, as well as steric constraints. We propose that the movement of the Phe330 ring, from the native perpendicular orientation to the parallel orientation, permits better accommodation of and protein−ligand interaction with the alkylene tethers of both (−)-**2a** and (−)-**2b** upon binding in the active gorge of *Tc*AChE, as seems to be also the case for E2020,[8] DECA[17] and the PEG200 molecule in the (−)-galanthamine complex.[11] In contrast, the perpendicularly oriented Phe330 ring observed in the *Tc*AChE complexes of (−)-HupA, EDR, and BW, appears to give optimum accommodation and strong nonpolar interactions with the respective ligands. If it were oriented parallel to the gorge axis, then it would present steric hindrance to ligand binding in the lower part of the gorge. The water networks around the **1a** units of both dimers at the bottom of the gorge are similar, and also quite similar to that around (−)-HupA at the catalytic anionic site, which was suggested to stabilize its complex with *Tc*AChE.[12] It was previously shown that (−)-HupA soaked into trigonal *Tc*AChE crystals occupies the sites of ca. seven conserved waters present in the native structure.[12,61] Likewise, superimposition of the initial electron density difference maps (Fo−Fc) of either the *Tc*AChE/(−)-**2a** or *Tc*AChE/(−)-**2b** structure onto the native structure (PDB code 2ACE), reveals that the dimer ligands displace ca. nine of the conserved water molecules.[61] Six of these waters are displaced by the $\mathbf{1a}_{cat}$ unit, one is displaced by the alkylene tether halfway up the gorge, and the remaining two are displaced by the $\mathbf{1a}_{per}$ moiety. Comparison of the native structure with the two *Tc*AChE/dimer structures also reveals that several gorge waters located in the latter structures (H_2O at equivalent positions 2, 3, 5, and 6, referred to in Table 4),[62] are not populated in the native structure. The fact that the two *Tc*AChE/dimer structures, determined independently, each show these same four H_2O peaks, implies that these may be the conserved gorge waters present in the native structure or poorly bound disordered waters which, rather than being displaced from the gorge, rearrange themselves within the active-site gorge upon binding of the dimers in order to favorably accommodate and interact with the dimer ligands (vide

(59) LSQ Explicit fit from residues 4−535, numbers in parentheses are the number of residue pairs LSQMAN used to calculate the rmsd values.
(60) Bourne, Y.; Taylor, P.; Bougis, P. E.; Marchot, P. *J. Biol. Chem.* **1999**, *274*, 2963−2970.
(61) Koellner, G.; Kryger, G.; Millard, C. B.; Silman, I.; Sussman, J. L.; Steiner, T. *J. Mol. Biol.* **2000**, *296*, 713−735.
(62) See Supporting Information.

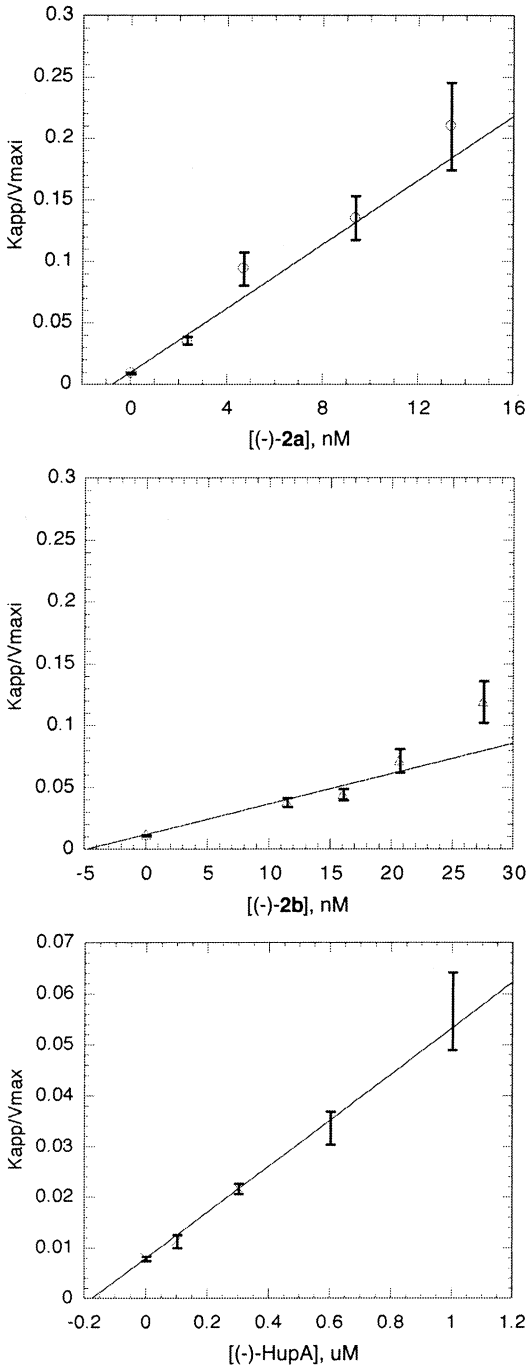

Figure 3. Steady-state inhibition of *Tc*AChE by (−)-**2a**, (−)-**2b**, and (−)-HupA. Values of v vs s at fixed concentrations of inhibitor, [I], were analyzed by use of the Henri-Michaelis−Menten equation. K_i values obtained by plotting the resulting values of K_{app}/V_{maxi} were plotted vs [I] in KaleidaGraph as previously described.[33] The graphs show the effect of (−)-**2a** (*top*), (−)-**2b** (*middle*) and (−)-HupA (*bottom*) on the K_{app}/V_{maxi} values for *Tc*AChE. Straight lines through the data points were fitted by weighted-least-squares minimization of the data, utilizing the expression of K_{app}/V_{maxi}, as derived for linear-mixed type inhibition (see the Experimental Section), taking the reciprocals of their variances as weights. STDs for each K_{app}/V_{maxi} value are shown as vertical bars.

infra). This phenomenon was earlier observed for the *Tc*AChE/E2020 complex.[8,61]

Protein−Ligand Interactions. The refined structures of *Tc*AChE/(−)-**2a** and *Tc*AChE/(−)-**2b** reveal very similar protein−ligand interactions. At the catalytic anionic site, the $\mathbf{1a}_{cat}$ unit of both dimers adopts the docking-predicted pseudoequatorial

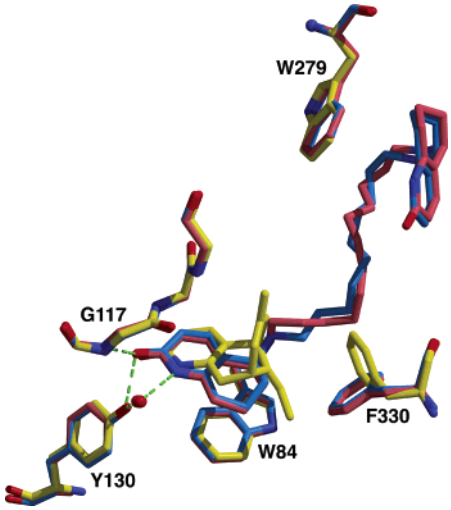

Figure 4. Overlay of the refined structures of *Tc*AChE/(−)-**2a** (sky blue), *Tc*AChE/(−)-**2b** (pink), and *Tc*AChE/(−)-HupA (yellow) showing the interactions of the catalytic site **1a** unit ($\mathbf{1a}_{cat}$) of (−)-**2b** with selected protein residues. Inhibitors and protein residues are rendered as sticks, and the water molecules shown as red spheres.

conformation at C-5 required for optimum binding,[29] and exhibits interactions similar to those seen in the *Tc*AChE/(−)-HupA complex.[12] These include hydrogen bonding interactions of the pyridone oxygen atom of the $\mathbf{1a}_{cat}$ moiety with Tyr130 O^{η} (2.7 Å) and Gly117 N (∼3.2−3.3 Å), and another hydrogen bond between the pyridone NH group of the $\mathbf{1a}_{cat}$ unit and a conserved water molecule, $H_2O(1)$ (2.9 and 2.7 Å for (−)-**2a** and (−)-**2b**, respectively) which, in turn, is hydrogen bonded to Glu199 $O^{\epsilon 1}$ (3.0 and 2.8 Å for (−)-**2a** and (−)-**2b**, respectively). The 5-amino group of the $\mathbf{1a}_{cat}$ unit of both dimers, which is likely to be protonated at the pH of the mother liquor (∼5.8), makes cation-π interactions with both the five-membered pyrrole ring of Trp84 and the aromatic ring of Phe330, with distances between the 5-amino nitrogen and the centroids of these rings of 5.2 and 4.9 Å, respectively, for (−)-**2a**, and 4.7 and 4.9 Å for (−)-**2b**. Moreover, the methine hydrogen at C-5 of the $\mathbf{1a}_{cat}$ moiety, which is predicted to bear some of the positive charge of the protonated 5-amino group,[11] also makes a cation-π binding interaction with the indole ring of Trp84, with distances between the C-5 carbon and the indole ring centroid of 4.0 and 3.8 Å for (−)-**2a** and (−)-**2b**, respectively. As expected from the high degree of structural similarity between the dimers and (−)-HupA (Figure 1), and from earlier docking studies of the HupA-like **1a** fragment,[29] the binding of either (−)-**2a** or (−)-**2b** to *Tc*AChE also invokes a peptide bond flip[63] between Gly117 and Gly118 at the catalytic anionic site, as seen in both the *Tc*AChE/(−)-HupA[12] and *Tc*AChE/(+)-HupA structures.[31] This peptide flip may partially account for the slow on rates of these dimers, as already suggested for (−)-HupA.[12,54]

From the $\mathbf{1a}_{cat}$ unit, the alkylene tether of both dimers snakes up the gorge toward the peripheral site $\mathbf{1a}_{per}$ unit, with a mixture of trans and gauche rotamers along its length. The protonated 5-amino group and the α-CH_2 group of the linker adjacent to the $\mathbf{1a}_{per}$ moiety, which is expected to carry part of the positive charge of the protonated 5-amino group,[11] both interact with

(63) Jones, T. A.; Zou, J.-Y.; Cowan, S. W.; Kjeldgaard, M. *Acta Crystallogr.* **1991**, *A47*, 110−119.

Table 4. Comparison of the Protein−Ligand Interactions of (−)-**2a**, (−)-**2b** and (−)-HupA with *Tc*AChE

entry	catalytic site contact partners		distances (Å) (–)-**2a**	(–)-**2b**	(–)-HupA[a]	interaction
	ligand	protein				
1	pyridone O[b]	Tyr130 O^{η}	2.73	2.66	2.59	H-bond
2	pyridone O[b]	Gly117 N	3.30	3.24	4.03	H-bond
3	5-amino N[c]	Trp84 (pyrrole)[g]	5.15	4.70	4.31	cation-π
4	5-amino N[c]	Phe330 (π-ring)[g]	4.92	4.88	4.79	cation-π
5	methine 5-C	Trp84 (indole)[g]	4.03	3.83	4.91	cation-π
6	α-CH_2 carbon	Phe330 (π-ring)[g]	3.81	5.48		cation-π
7	C═C (sp^2, 12-C)[d,f]	Trp84 (indole)[g]			3.84	$\pi-\pi$ stacking
8	C═C (sp^2, 12-C)[d,f]	Phe330 (π-ring)[g]			4.17	$\pi-\pi$ stacking
9	ethylidene (sp^3 C)[e,f]	His440 O			2.98	C−H···O, H-bond
	ligand	water				
10	pyridone N	$H_2O(1)$[h]	2.90	2.74	3.02	H-bond
11	5-amino N[c]	$H_2O(2)$[h]	3.24	2.96	3.07	H-bond
12	5-amino N[c]	$H_2O(3)$[h]	2.67			H-bond
13	α-CH_2 carbon	$H_2O(3)$[h]		2.05		close contact
	water	protein				
14	$H_2O(1)$[h]	Glu199 $O^{\epsilon 1}$	2.96	2.80	2.81	H-bond
15	$H_2O(3)$[h]	Tyr121 O^{η}	2.68	2.67		H-bond
16	$H_2O(3)$[h]	Ser122 O^{γ}	3.07	3.25		H-bond

	peripheral site contact partners		distances (Å) (–)-**2a**	(–)-**2b**	interaction
	ligand	protein			
17	pyridone O[b]	Phe288 N	2.67	2.74	H-bond
18	5-amino N[c]	Trp279 (indole)[g]	5.01	5.32	cation-π
19	α-CH_2 carbon	Trp279 (indole)[g]	3.57	3.92	cation-π
	ligand	water			
20	pyridone N	$H_2O(4)$[h]	2.67	2.88	H-bond
21	5-amino N[c]	$H_2O(5)$[h]	2.78	2.56	H-bond
22	5-amino N[c]	$H_2O(6)$[h]	2.77	2.92	H-bond
	water	protein			
23	$H_2O(4)$[h]	Arg289 O	2.72	2.77	H-bond
24	$H_2O(4)$[h]	Arg289 N	2.89	2.99	H-bond
25	$H_2O(4)$[h]	Ser286 O^{γ}	3.32	3.16	H-bond

[a] From PDB code 1VOT.[12] [b] Carbonyl oxygen of the pyridone ring. [c] Unlike (−)-HupA, which has a primary amine, (−)-**2a** and (−)-**2b** have a secondary amine at the corresponding position. [d] Ethylidene sp^2 carbon at position 12 of (−)-HupA. [e] The main-chain carbonyl oxygen of His440 interacts with (−)-HupA through its ethylidene-methyl group at position 13 (numbering as in Figure 1).[12] [f] (−)-**2a** and (−)-**2b** have no ethylidene C═C or CH_3 group at these positions. [g] Distances to the centroid of designated aromatic rings. [h] See Table S1 in Supporting Information for assignment of equivalent water molecules.

the indole ring of the peripheral site tryptophan residue, Trp279, in a cation-π interaction. Distances between these nitrogen and carbon atoms and the centroid of the indole ring of Trp279 are 5.0 and 3.6 Å, respectively, for (−)-**2a**, and 5.3 and 3.9 Å, respectively, for (−)-**2b**. Unexpectedly, this $\mathbf{1a}_{per}$ unit then appears to curl back upon itself into the gorge, in the lower energy pseudoaxial conformation at C-5,[29] and forms a hydrogen bond between its pyridone oxygen and Phe288 N (2.7 Å).[62] The pyridone NH groups of the $\mathbf{1a}_{per}$ moiety of both dimers form hydrogen bonds with a conserved water molecule, $H_2O(4)$ (2.7 and 2.9 Å for (−)-**2a** and (−)-**2b**, respectively), which in turn is hydrogen bonded to the main chain carbonyl oxygen of Arg289 (2.7 and 2.8 Å for (−)-**2a** and (−)-**2b**, respectively). The protonated 5-amino group of both dimers appears to hydrogen bond to two proximal water molecules, $H_2O(5)$ and $H_2O(6)$ (∼2.6−2.9 Å, equivalent water molecules referred to in Table 4, entries 21 and 22),[62] near the opening of the gorge (vide supra). The protein−ligand interactions of *Tc*AChE with (−)-**2a**, (−)-**2b** and (−)-HupA are summarized in Table 4.

The $\mathbf{1a}_{cat}$ moieties of both HupA-like dimers exhibit hydrophobic interactions with the six-membered benzene ring of Trp84, at the catalytic anionic site, where the six-membered ring carbons of the indole of Trp84 are within 3.4−4.0 Å of most of the cyclohexene ring atoms. Moreover, both dimers also appear to make favorable hydrophobic contacts with the side chains of several aromatic residues along the gorge via the alkylene tether, with most of the tether carbons being within 3.4−4.0 Å of the aromatic ring carbons. Such interactions are made with the rings of Phe330 and Phe331, in the lower part of the gorge, and with those of Tyr70, Trp279, and Tyr334, near its opening. A similar ligand-binding pattern was reported for structures of the complexes of *Tc*AChE with E2020 and DECA (PDB codes 1EVE and 1ACL, respectively), in which the inhibitors bind analogously to these same aromatic residues lining the gorge;[8,17,61] in contrast, the recently determined structure of *Tc*AChE with BW (PDB ID 1E3Q)[19] shows the inhibitor tracing the opposite wall in the lower part of the gorge, toward Ser200, Gly118, Gly119, and Phe290, as is also the case for DECA in "native" mAChE (PDB ID 1MAA)[60] as noted above. Although the difference in the ligand binding pattern of the BW complex may be attributed to hydrogen bonding interactions made by the BW carbonyl oxygen with Tyr121 O^{η} (3.5 Å) and Phe290 $C^{\epsilon 1}$ (3.0 Å; O···H−C type), the inverted curvature of DECA in the "native" mAChE in the lower part of the gorge, relative to *Tc*AChE, is due to steric hindrance by the perpendicularly oriented Tyr337 ring.[60]

In general, the X-ray results show that the longer dimer, (−)-**2b** (twelve-carbon spacer), makes stronger hydrogen bonding contacts at the catalytic anionic site between its $\mathbf{1a}_{cat}$ moiety and Tyr130 O^{η}, Gly117 N, and Glu199 $O^{\epsilon 1}$, through a water

molecule, $H_2O(1)$, than its shorter tether homolog, (−)-**2a** (ten-carbon spacer), i.e., 2.7, 3.2, 2.7, and 2.8 Å, respectively for (−)-**2b**, and 2.7, 3.3, 2.9 and 3.0 Å, respectively, for (−)-**2a** (Table 4, entries 1, 2, 10, and 14). In contrast, (−)-**2a** exhibits stronger hydrogen bonding between its $\mathbf{1a}_{per}$ moiety and Arg289 O (through a water molecule, $H_2O(4)$) (2.7 and 2.7 Å, respectively for (−)-**2a**, and 2.9 and 2.8 Å respectively for (−)-**2b**; Table 4, entries 20 and 23), as well as a stronger cation-π interaction with the indole moiety of Trp279 at the peripheral anionic site (5.0 and 3.6 Å, respectively, for (−)-**2a**, and 5.3 and 3.9 Å respectively for (−)-**2b**; Table 4, entries 18−19). There is also a significant difference in the mode of cation-π binding between (−)-**2a** and (−)-**2b** in the vicinity of the catalytic site. The methine hydrogen at C-5 and the α-CH_2 group of the $\mathbf{1a}_{cat}$ units of both dimers are expected to carry part of the positive charge of the protonated 5-amino group.[11] Although (−)-**2b** has the closest approach of its 5-amino N and methine 5-C to the π-system of Trp84 (Table 4, entries 3 and 5), (−)-**2a** has the closest approach of its α-CH_2 carbon to the ring centroid of Phe330 (3.8 Å for (−)-**2a**, compared to 5.5 Å for (−)-**2b**, Table 4, entry 6). This latter difference in distance is quite significant, as clearly seen in Figure 4. We thus suggest that this may be the decisive factor responsible for the higher affinity observed of *Tc*AChE for (−)-**2a** relative to (−)-**2b** (∼6−7-fold, Table 1). This difference in the mode of cation-π binding appears to be a consequence of the difference in tether length. Two gorge water molecules, $H_2O(2)$ and $H_2O(3)$,[62] are located at identical positions in the same catalytic anionic region in both the *Tc*AChE/ (−)-**2a** and *Tc*AChE/(−)-**2b** structures, whereas the protonated 5-amino group of the $\mathbf{1a}_{cat}$ unit of (−)-**2a** makes hydrogen bonds with both these proximal waters (3.2 and 2.7 Å respectively, Table 4, entries 11 and 12). The difference in the linker disposition permits a hydrogen bond of only one of these water molecules, $H_2O(2)$, with the 5-amino group of the $\mathbf{1a}_{cat}$ unit of (−)-**2b** (3.0 Å; Table 4, entry 11). Concerning the second water molecule, $H_2O(3)$, which is associated with Tyr121 O^{η} (2.7 Å) and Ser122 O^{γ} (3.3 Å), it appears to be near the α-CH_2 carbon (2.0 Å) of the $\mathbf{1a}_{cat}$ moiety of (−)-**2b** (Table 4, entry 13). We describe this as a nonbonding close contact, which may arise from rearrangement of the gorge waters upon binding of (−)-**2b** (vide supra). In particular, we suggest that the water molecule at equivalent position 3 in both *Tc*AChE/dimer structures may correspond to H_2O 633 in the native *Tc*AChE structure (PDB ID 2ACE[12]).[61,62] This type of water redistribution and subsequent ligand and protein interaction has also been suggested previously for other inhibitors, such as E2020.[8,61]

Discussion

The inhibition potency values displayed in Table 1 clearly show that both HupA-like dimers, (−)-**2a** and (−)-**2b**, bind more tightly than (−)-HupA to *Tc*AChE (> 170- and ≥26-fold, respectively). Their enhanced potency, relative to the pharmacologically inactive monomer **1a**, is consistent with the crystallographic data for the two *Tc*AChE/dimer complexes, which clearly reveal, as predicted,[29] binding of one HupA-like **1a** moiety to the "anionic" subsite of the active-site similarly to (−)-HupA,[12] and the other to the peripheral "anionic" site (see Table 4). Overlay of the X-ray structures of *Tc*AChE with (−)-**2a**, (−)-**2b**, and (−)-HupA (Figure 4) reveals that both dimers make cation-π and hydrogen bonding interactions at the peripheral anionic site which can contribute to their enhanced affinity relative to the (−)-HupA monomer (see Table 4, entries 17−25).[62] Our data suggest that the interactions made by the $\mathbf{1a}_{per}$ unit of both dimers, which the tether provides at minimal entropic cost,[24] may substantially compensate for the weaker and/or missing interactions of the $\mathbf{1a}_{cat}$ unit, relative to (−)-HupA, in the vicinity of the catalytic anionic site of *Tc*AChE. These include the following: (i) a weaker cation-π interaction of the protonated 5-amino group of the $\mathbf{1a}_{cat}$ moieties in both dimers with the aromatic π-systems of Trp84 and Phe330 (Table 4, entries 3 and 4); (ii) the lack of $\pi-\pi$ stacking interactions seen between the ethylidene π-system of (−)-HupA, which is absent in both (−)-**2a** and (−)-**2b** (see Figure 1), and the aromatic rings of Trp84 and Phe330 (Table 4, entries 7−8);[12] and (iii) the absence of the hydrogen bonding seen between the ethylidene methyl group of (−)-HupA and the main chain His440 O for both dimers (Table 4, entry 9).[12] A principal point to be emphasized, based on the structures of the two complexes, apart from the difference in tether conformation seen for the $\mathbf{1a}_{cat}$ unit between (−)-**2a** and (−)-**2b** in the lower part of the gorge, is that there is little difference in overall conformation between the two. How can the preference of *Tc*AChE for (−)-**2a** over (−)-**2b** be rationalized? It is clear that both dimers bind to *Tc*AChE in a bivalent manner. Reduced entropy loss on binding would favor the shorter tether ((−)-**2a**), but if this factor were dominant, the (−)-**2a**/(−)-**2b** potency order would not be reversed for rat AChE. A reduced desolvation penalty could likewise explain the preference of rat AChE for the longer dimer (−)-**2b**, but cannot explain the preference of *Tc*AChE for the shorter one, (−)-**2a**. It thus appears that the preference of *Tc*AChE for (−)-**2a**, and the preference of rat AChE for (−)-**2b**, is due in each case to greater protein−ligand complementarity.

It is well established that *Tc*AChE and mammalian (human, mouse) AChEs, and their complexes with various inhibitors, display a high degree of sequence and structural similarity, especially with respect to their active-site gorge.[60,62,64] Thus, subtle structural differences in the active-site gorges between different species of AChE have been proposed to play a role in determining selectivity for substrates and inhibitors (e.g., (−)-HupA, tacrine, EDR, and DECA with respect to *Tc*AChE and FBS AChE).[55] This proposal is supported by the larger C_α rmsd values generally found between structures of AChEs from different species (overall > 0.7 Å, gorge > 0.5 Å; *Torpedo*, mouse and human AChEs) (see, for example, Lit.[55,64−66]), relative to the smaller C_α rmsd values between structures of AChEs from the same species and their complexes with inhibitors (overall < 0.6 Å, gorge < 0.5 Å) (see, for example, Lit.[55,60,64,66]).[67] In addition, the presence of Tyr337 in mammalian AChEs has been proposed to contribute to the higher binding affinity and stabilization of (−)-HupA to mammalian AChEs and their mutants than to *Tc*AChE.[30,54−56] This is achieved principally through the enhanced cation-π interactions

(64) Kryger, G.; Harel, M.; Giles, K.; Toker, L.; Velan, B.; Lazar, A.; Kronman, C.; Barak, D.; Ariel, N.; Shafferman, A.; Silman, I.; Sussman, J. L. *Acta Crystallogr.* **2000**, *D56*, 1385−1394.
(65) Bourne, Y.; Taylor, P.; Marchot, P. *Cell* **1995**, *83*, 503−512.
(66) Felder, C. E.; Botti, S. A.; Lifson, S.; Silman, I.; Sussman, J. L. *J. Mol. Graphics & Modelling* **1997**, *15*, 318−327.
(67) Rmsd values for C_α atoms were determined using the Explicit fit utility of LSQMAN (ref 51). Range of overall residues used (527): 4−107, 108−259, 260−484, and 490−535 for *Tc*AChE; and 6−109, 111−262, 267−491, and 498−543 for mAChE or hAChE. For a list of active-site gorge residues used (42), see Table S2 in Supporting Information.

between the ammonium group of (−)-HupA and the phenol ring of Tyr337, relative to Phe330 in *Tc*AChE (see, for example, Lit.[16,17,68,69]), the hydroxyl group of Tyr337 forming a hydrogen bond with the ammonium group of (−)-HupA,[12,16,33] and possibly through the enhanced $\pi-\pi$ interaction of the Tyr337 ring with the ethylidene π-system of (−)-HupA.

Although no crystal structure of rat AChE has yet been solved, the amino acid sequence of rat AChE, as derived from the mRNA sequence, is virtually identical to that of mAChE (98% identity, 99% homology).[70,71] We, therefore, considered it appropriate to use the mAChE structure (PDB ID 1MAA),[60] which contains a bound DECA molecule, as a model to explore the subtle structural differences within their active-site gorges that may account for the species-dependent differences in specificity seen for (−)-**2a-b**, (−)-HupA, and other inhibitors (see, for example, Lit.[72]). Superimposition of the C_α atoms of Trp86 and Trp286 in the mAChE structure (PDB ID 1MAA)[60] on those of the corresponding Trp84 and Trp279 residues in native and DECA bound *Tc*AChE (PDB ID 2ACE[12] and 1ACL,[17] respectively), reveals three major differences between the active-site gorges of these enzymes, which may prove crucial for understanding the species-dependent differences in specificity of AChEs for substrates and inhibitors. First, the lower part of the gorge of mAChE is much narrower than of *Tc*AChE. Not only is the Tyr341 ring (corresponding to Tyr334 in *Tc*AChE) in the mAChE structure shifted toward the center of the gorge, ∼1.5 Å removed from its position in *Tc*AChE, as previously reported,[60] but the C_α positions of Tyr337 and Phe338 in mAChE are shifted ca. 1 Å away from those of the corresponding Phe330 and Phe331 residues, respectively, in the *Tc*AChE structures, also toward the center of the gorge. This is also the case for the Fas2 complexes of mAChE and hAChE.[64,65] Second, as mentioned earlier, the steric effects of the Tyr337 ring appear to be responsible for the inverted curvature adopted by the DECA molecule in the lower part of the gorge of mAChE, relative to that seen in the *Tc*AChE structure.[60] The perpendicular alignment of the Tyr337 ring with respect to the gorge axis in mAChE, which is similarly observed in the hAChE/Fas2 and mAChE/Fas2 structures (PDB codes 1B41 and 1MAH, respectively)[64,65] appears to be intrinsic to these mammalian AChEs. In contrast, the homologous Phe330 ring lies parallel to the gorge axis in the *Tc*AChE/DECA complex (PDB ID 1ACL), whereas in the *Tc*AChE/Fas2 complex (PDB ID 1FSS), in the native *Tc*AChE structure and in its complexes with other inhibitors,[8] such as *Tc*AChE/(−)-HupA (PDB ID 1VOT),[12] the Phe330 ring lies perpendicular to the gorge axis. Third, the Tyr337 residue in mAChE and hAChE is conformationally restricted compared to *Tc*AChE Phe330. The mAChE and hAChE structures reveal a hydrogen bonding interaction between the hydroxyl groups of Tyr337 and Tyr341 within the active-site gorge (up to ∼3.5 Å),[60,64,65] which is lacking in *Tc*AChE. It is likely that this hydrogen bonding of the Tyr337 residue seen in mammalian AChEs serves to restrict its conformational flexibility when compared to *Tc*AChE Phe330. As a result, mammalian AChE Tyr337 cannot easily adopt the versatile "swinging gate" conformations seen for Phe330 in *Tc*AChE and in its complexes with various inhibitors,[8] thus rendering it less accommodating than *Tc*AChE to certain inhibitors.

These structural differences between the gorges of mAChE structure and *Tc*AChE, are consistent with the enhanced potency and selectivity reported for (−)-HupA in mammalian AChEs. (−)-HupA binding is not adversely affected by the perpendicular alignment of Tyr337. Its high affinity for mammalian AChE is most likely due both to closer protein−ligand contacts arising from the narrowness of their gorge, and to the proposed hydrogen bonding with Tyr337 O^η. It is also likely that the Tyr337 residue similarly forces a different pathway for the alkylene tether of both (−)-**2a** and (−)-**2b** along the gorge of rat AChE than that observed in the *Tc*AChE complex structures determined herein, both by its steric and polar contributions, as indeed is seen for the DECA molecule in the mAChE structure.[60] The tighter binding of (−)-**2b** relative to (−)-**2a** (∼3-fold; Table 1) with rat AChE,[29] may thus arise from the optimum binding of both **1a** units of (−)-**2b** to both catalytic and peripheral anionic sites, and from the higher degree of conformational flexibility of its longer 12-carbon tether because this would permit greater protein−ligand complementarity for (−)-**2b** than for the shorter 10-carbon analogue, (−)-**2a**. Moreover, the crystallographic data show that (−)-**2a** is already more fully stretched in the gorge of *Tc*AChE than (−)-**2b**. We attribute the marginal potency difference seen between dimers (−)-**2a** and (−)-**2b** and (−)-HupA for rat AChE (less than 3-fold; Table 1) to the higher specificity and affinity of rat AChE for (−)-HupA relative to the dimers, and to the destabilizing steric effects of Tyr337 on the binding of (−)-**2a** and (−)-**2b**, as described above. Conversely, the absence of Tyr337 stabilization of (−)-HupA binding to *Tc*AChE, as well as the reduced steric effect of Phe330 on the binding of the dimers, result in the comparatively larger dimer/(−)-HupA inhibition potency ratios observed for *Tc*AChE (see Table 1).

Conclusions

The crystallographic data show that the HupA-like bivalent dimers, (−)-**2a** and (−)-**2b**, indeed bind within the gorge of *Tc*AChE in a bivalent fashion, with one **1a** unit bound to the catalytic anionic site and the other to the peripheral anionic site, and that their enhanced affinity for *Tc*AChE relative to (−)-HupA is conferred by dual-site binding and operation of the chelate effect. The (*S*)-$\mathbf{1a}_{cat}$ units of the dimers bind similarly to (−)-HupA, despite their absolute configuration being reversed, while the $\mathbf{1a}_{per}$ unit binds via cation-π as well as hydrogen bonding. Unexpectedly, the optimal tether length for the dimers differs between *Tc*AChE and rat AChE: (−)-**2a** interacts better in *Tc*AChE and (−)-**2b** in rat AChE. On the basis of the closely related mAChE structure (PDB ID 1MAA), the differences in inhibition potency can be ascribed to the smaller gorge dimensions of rat AChE, as well as to the steric and polar contributions of Tyr337 in rat AChE, relative to the equivalent Phe330 residue in *Tc*AChE. Thus, the crystal structures permit rationalization of the presently reported inhibition data obtained for (−)-HupA, (−)-**2a** and (−)-**2b** on *Tc*AChE, and those previously reported on rat AChE.[29] They

(68) Verdonk, M. L.; Boks, G. J.; Kooijman, H.; Kanters, J. A.; Kroon, J. *J. Comput.-Aided Mol. Des.* **1993**, *7*, 173−182.
(69) Felder, C.; Jiang, H.-L.; Zhu, W.-L.; Chen, K.-X.; Silman, I.; Botti, S. A.; Sussman, J. L. *J. Phys. Chem. A* **2001**, *105*, 1326−1333.
(70) Rachinsky, T. L.; Camp, S.; Li, Y.; Ekström, J.; Newton, M.; Taylor, P. *Neuron* **1990**, *5*, 317−327.
(71) Legay, C.; Bon, S.; Massoulié, J. *FEBS Lett.* **1993**, *315*, 163−166.
(72) Kraut, D.; Goff, H.; Pai, R. K.; Hosea, N. A.; Silman, I.; Sussman, J. L.; Taylor, P.; Voet, J. G. *Mol. Pharmacol.* **2000**, *57*, 1243−1248.
(73) Laskowski, R. A.; MacArthur, M. W.; Moss, D.; Thornton, J. M. *J. Appl. Crystallogr.* **1993**, *26*, 283−291.

serve to increase our understanding of the species-dependent differences in specificity of mammalian AChE for other substrates and inhibitors, which is of crucial importance to future drug development in the area under investigation.

Acknowledgment. This project was supported by the Research Grants Council (HK) Competitive Earmarked Research Grants HKUST6236/99M and HKUST6120/02M, the Alzheimer's and Related Disease Award Fund (Commonwealth of Virginia, 03-1), the U.S. Army Medical and Material Command under Contract No. DAMD17-97-2-7022, the EC 5th Framework Program on the Quality of Life and Management of Living Resources, the Kimmelman Center for Biomolecular Structure and Assembly (Rehovot, Israel), and the Benoziyo Center for Neurosciences. I.S. is the Bernstein-Mason Professor of Neurochemistry. J.L.S. is the Pickman Professor of Structural Biology. We thank Meryl A. Sava, David Shaya, and Lilly Toker for help in this research, and Terrone L. Rosenberry (Mayo Clinic Jacksonville) for valuable discussions.

Supporting Information Available: 1. Additional discussion of sequence and structural comparisons made between *Tc*AChE and mammalian AChE; 2. Tables for equivalent water molecules in the active-site gorge of *Tc*AChE complexes, and list of active-site gorge residues in *Tc*AChE and mammalian AChEs used for structural comparison; and 3. Additional illustrations of the binding interactions of (−)-**2a** in the active-site gorge of *Tc*AChE. All this material is available free of charge via the Internet at http://pubs.acs.org.

JA021111W